coatings

MDPI

Article

Fabrication and Performance of Durable Superhydrophobic Cement Mortar by Combining Dry Modification with Stearic Acid and Template Molding

Ying Zhai [1], Huiru Chen [2], Haojie Wu [2], Defeng Yan [2], Zhanbin Gu [3] and Shuwei Lv [3,*]

[1] School of Mechanical Engineering, Changchun Guanghua University, Changchun 130033, China; zhaiying90@163.com
[2] College of Mechanical and Electronic Engineering, Nanjing Forestry University, Nanjing 210037, China; yandefeng@njfu.edu.cn (D.Y.)
[3] School of Mechanical and Vehicle Engineering, Jilin Engineering Normal University, Changchun 130052, China
* Correspondence: lv0529@126.com

Abstract

Cement mortar is widely used in buildings, roads, bridges, and other infrastructure. However, its inherent porous structure and hydrophilicity facilitate the penetration of water and aggressive media into the cement mortar matrix, accelerating rebar corrosion and compromising structural durability. The construction of superhydrophobic cement mortar surfaces can effectively improve water repellency, self-cleaning performance, antifouling performance, and corrosion resistance. However, existing superhydrophobic cement mortar surfaces have several limitations, such as complex fabrication processes, susceptibility to mechanical damage, and inadequate mechanical durability of surface coatings. To address these limitations, we propose a method for preparing superhydrophobic cement mortar that combines dry modification with stearic acid and template molding. Cement was hydrophobically modified with stearic acid, and a nylon mesh template was used to construct rough structures during cement mortar molding. The prepared superhydrophobic cement mortar exhibited excellent water repellency, self-cleaning performance, and antifouling properties, as well as good repellency to various water-soluble liquids. Moreover, the superhydrophobic surface retained good hydrophobicity after sandpaper abrasion and sand impact tests, indicating good mechanical stability. Furthermore, the superhydrophobic structure can effectively hinder the penetration of water and corrosive media into the cement matrix, improving the corrosion resistance of the cement mortar. The method features a simple fabrication process, avoids the use of fluorinated low-surface-energy agents, and offers tunability in surface appearance, providing a feasible route for preparing superhydrophobic cement mortar that integrates waterproofing, self-cleaning, antifouling, corrosion resistance, and decorative functions.

Keywords: superhydrophobic; cement mortar; dry modification; template molding; mechanical durability

Check for updates

Academic Editor: Valeria Vignali

Received: 5 September 2026
Revised: 5 October 2026
Accepted: 8 October 2026
Published: 10 October 2026

Copyright: © 2026 by the authors. Licensee MDPI, Basel, Switzerland. This article is an open access article distributed under the terms and conditions of the Creative Commons Attribution (CC BY) license.

1. Introduction

Cement mortar is widely used in buildings, roads, bridges, hydraulic structures, and marine engineering owing to the widespread availability of its raw materials, favorable mechanical properties, and relatively low cost [1,2]. However, hardened cementitious

materials typically contain capillary pores, gel pores, and microcracks, while their hydration products contain hydrophilic surface groups, resulting in a strong affinity for water [3,4]. During service, water can act as a transport medium for chloride ions, sulfate ions, and other aggressive species to penetrate the cementitious matrix, potentially inducing steel corrosion, sulfate attack, freeze–thaw damage, and salt crystallization, thereby degrading material performance and shortening the service life of structures [5–7]. Therefore, reducing the affinity of cementitious materials for water and restricting the transport of liquid water and aggressive species are important for improving their durability.

Inspired by natural water-repellent surfaces, such as lotus and rice leaves, superhydrophobic surfaces can be constructed through the combination of low-surface-energy chemical components and appropriate micro/nanoscale roughness and are generally characterized by a water contact angle greater than 150° and a low rolling angle [8,9]. In the Cassie–Baxter wetting state, air can be trapped between a water droplet and the rough solid surface, thereby reducing the actual solid–liquid contact area and suppressing direct contact between water and the substrate. Based on this wetting mechanism, superhydrophobic cementitious materials can exhibit not only strong water repellency but also self-cleaning, antifouling, and corrosion-protection properties, making them attractive for the surface protection of cementitious materials [10]. Superhydrophobic cementitious surfaces are generally constructed by combining low-surface-energy chemical modification with appropriate surface roughness. Common approaches include spraying or coating, impregnation, incorporation of hydrophobic components, and template-assisted surface structuring [11]. Coating and spraying can introduce low-surface-energy functional layers onto cementitious substrates, while micro/nanoparticles can be incorporated to generate multiscale surface roughness. However, these surface functional layers may be damaged or detached under mechanical abrasion or particle impact, resulting in the deterioration of their water repellency. Impregnation can modify the surface properties of pore walls within a certain penetration depth, although its effectiveness depends strongly on the penetration capability of the modifier and the pore structure of the substrate. Incorporating hydrophobic components into cementitious systems can extend the distribution of hydrophobic species beyond the outermost surface, but it may simultaneously affect cement hydration, pore structure, and mechanical properties [12]. Therefore, the development of superhydrophobic cementitious materials requires consideration of not only surface chemistry and surface morphology but also of the preparation route, basic properties of the matrix, and mechanical stability of the resulting superhydrophobic surface.

Fatty carboxylic acids, which contain a polar carboxyl group and a nonpolar long-chain alkyl group, have attracted attention as low-surface-energy modifiers for cementitious materials. The carboxyl group can interact with calcium-containing species in cementitious systems, whereas the long hydrocarbon chain contributes to a reduction in surface free energy. Albayrak et al. investigated the effects of several fatty acids, including oleic, stearic, myristic, and lauric acids, on cement and concrete, demonstrating that the type and dosage of fatty acids can influence the properties of cementitious materials [13]. In addition to their direct application to cementitious materials, fatty acids have been used for the pre-modification of inorganic powders. Spathi et al. modified paper sludge ash with fatty acids through dry grinding and demonstrated that long-chain fatty acids could impart pronounced hydrophobicity to inorganic powders [14]. Liu et al. modified fly ash with oleic acid and subsequently incorporated the modified powder into Portland cement, demonstrating the feasibility of regulating the water absorption behavior of cementitious materials through fatty-acid-modified mineral powders [15]. Furthermore, Chen et al. investigated the hydrophobic modification of cement-based materials using a long-chain carboxylic acid through experimental and molecular-scale analyses, providing insight into

the influence of carboxylic acids on interfacial wetting and water transport in cement hydration products [16]. These studies demonstrate that fatty carboxylic acids can effectively regulate the interfacial properties of cementitious materials and related inorganic powders, although their effects depend on the type of carboxylic acid, the substrate being modified, and the method by which the modifier is introduced.

Stearic acid (STA) is a saturated C18 fatty carboxylic acid whose carboxyl group can interact with calcium-containing species in cementitious systems, while its long alkyl chain contributes to lowering the surface free energy. STA has therefore been employed for the hydrophobic modification of cementitious materials, and previous studies have demonstrated its ability to reduce water absorption and enhance surface hydrophobicity [17–21]. Existing studies have predominantly introduced STA through wet-processing routes, such as solution impregnation and emulsion treatment, which generally involve the dissolution or dispersion of the modifier, liquid-phase treatment, and subsequent drying [22–24]. In contrast, directly modifying cement powder with STA through a dry process before mortar preparation enables the surface chemistry of cement particles to be tailored at the powder stage while avoiding an additional liquid-phase modification step. Subsequently, covering the fresh mortar surface with a nylon mesh template enables regular microstructures to be replicated during molding, thereby combining low-surface-energy modification at the cement-powder stage with surface roughness construction at the mortar-forming stage [25–28]. This combined strategy provides a preparation route distinct from conventional wet STA treatment by integrating chemical modification of cement powder with template-induced surface structuring, and its effects on the wetting behavior, mechanical stability, and matrix properties of cement mortar warrant further investigation.

Based on the above considerations, this study aims to construct superhydrophobic cement mortar by combining dry modification of cement powder with STA and nylon-mesh-assisted surface microstructures and to systematically evaluate its wetting behavior and related properties. First, STA was directly applied to cement powder through thermomechanical mixing to obtain hydrophobically modified cement. The modified cement was subsequently used to prepare mortar, and a nylon mesh template was placed on the fresh mortar surface to replicate regular microstructures, thereby combining low-surface-energy modification at the powder stage with surface roughness construction during mortar forming. Different modification conditions and corresponding control groups were employed to distinguish the effects of STA modification and nylon-mesh-induced surface structures on the wetting behavior of the mortar, while surface morphology and chemical characterization were used to investigate the formation mechanism of the superhydrophobic surface. In addition, the basic physical and mechanical properties, self-cleaning and antifouling performance, mechanical durability, and protective performance of the modified mortar were evaluated. This study is intended to provide a research foundation for the preparation and performance regulation of superhydrophobic cementitious materials.

2. Experimental Section

2.1. Materials

Ordinary Portland cement (PO 42.5) was purchased from Jilin Yatai Cement Co., Ltd. (Changchun, China). Fine aggregate was fine sand with a particle size not exceeding 300 μm. Stearic acid (STA, $CH_3(CH_2)_{16}COOH$) was purchased from Jiangsu Haian Petrochemical Plant (Nantong, China). A nylon mesh with a mesh size of 300 μm, which was used as a template for constructing the microstructures, was purchased from Guangzhou Hualong Screen Mesh Industrial Co., Ltd. (Guangzhou, China).

2.2. Preparation of the Superhydrophobic Cement (S-Cement)

Stearic acid-modified superhydrophobic cement, denoted as S-cement, was prepared via a one-step dry process using a mixer (SHR10L-B, Keren Machinery Co., Ltd. (Changchun, China)). First, 75 g of ordinary Portland cement was added to the mixer. The cement was preheated at 65 °C and mixed at 1100 r/min for 15 min to minimize the influence of adsorbed water on the cement powder during subsequent surface modification. Then, 2 g of stearic acid was added to the cement. The mixture was mixed at 1100 r/min at 75 °C for 25 min. After the dry modification process, stearic acid-modified cement powder was obtained. In this solvent-free dry process, high-speed mechanical mixing promoted the uniform dispersion of stearic acid on the surfaces of cement particles, while moderate heating facilitated interfacial interactions between stearic acid and calcium-containing active sites on the cement surface, contributing to the formation of a low-surface-energy organic layer [29].

2.3. Preparation of the Superhydrophobic Cement Mortar (SHP-C)

The prepared S-cement, fine sand, and water were added to a beaker at a mass ratio of 1:1:0.5 and mechanically mixed at 200 r/min for 5 min using an electric mixer to obtain a homogeneous mortar mixture. Subsequently, the fresh mixture was poured into molds with dimensions of 20 mm × 20 mm × 5 mm. A nylon mesh with a mesh size of 300 μm was placed on the upper surface of the sample to serve as a template for constructing the rough surface texture. The molded sample was initially cured under laboratory conditions at 25–28 °C and a relative humidity of 30%–60% for 24 h. Afterward, the nylon mesh was removed from the sample. Curing was then continued under the same conditions for a total curing time of 3 d, at which point the sample was named SHP-C. The overall preparation process is shown in Figure 1. For comparison, ordinary Portland cement mortar (O-C) was prepared as a reference sample with a mixing proportion, molding procedure and curing conditions similar to those of SHP-C.

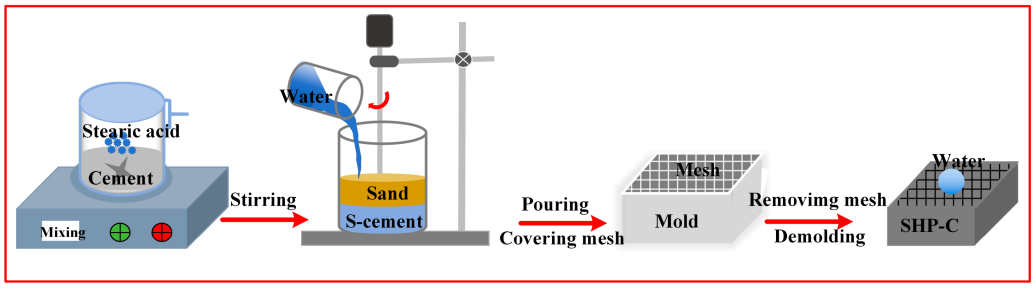

Figure 1. Schematic illustration of the preparation process of SHP-C.

2.4. Characterization

The surface micromorphology and microstructures of the samples were observed using a scanning electron microscope (SEM, SU3500, Hitachi High-Tech, Tokyo, Japan). The water contact angle (CA) and rolling angle (RA) were measured using a contact angle measuring instrument (DSA-100, KRÜSS GmbH, Hamburg, Germany). A water droplet of approximately 5 μL was used for the CA measurement. For the RA measurement, a water droplet of approximately 10 μL was placed on the initially horizontal sample surface, and the sample stage was manually tilted slowly and continuously at a speed of about 0.2°/s. The inclination angle at which the droplet began to roll across the surface was recorded as the RA. For all samples, the CA and RA values were measured at least five times at randomly selected positions [30,31].

2.5. Self-Cleaning and Antifouling Tests

The self-cleaning performance of SHP-C was evaluated using chalk dust as a simulated solid contaminant. First, identical amounts of chalk dust were uniformly distributed over the surfaces of O-C and SHP-C. Subsequently, the samples were tilted at about 15°, and water droplets were dripped onto the surfaces to observe the entrainment and removal of chalk dust by rolling droplets. To evaluate the liquid contaminant repellency of SHP-C, the samples were tilted at approximately 10°, and various water-soluble liquids, including tea, ink, simulated seawater (3.5 wt% NaCl aqueous solution), muddy water, cola, coffee, milk, and juice, were used for testing. The contact angles and rolling angles of these liquids on the SHP-C surface were measured, and the residual contamination on the sample surface after droplet rolling was observed [32].

2.6. Sandpaper Abrasion Test

To evaluate the mechanical durability of SHP-C, the sample was placed with its superhydrophobic surface facing downward onto 800# sandpaper, and a 200 g weight was placed on top of the sample to provide a constant load. The sample was then manually moved horizontally along the sandpaper surface; the sliding speed was not quantitatively controlled or recorded, with every 20 cm of abrasion distance defined as one abrasion cycle. After each cycle, the CA and RA of the sample were measured to evaluate the changes in superhydrophobic performance during the abrasion process [33].

2.7. Sand Impact Test

The SHP-C sample was fixed on a platform with a 20° inclination angle. Sea sand with a particle size of about 1 mm was used as the impact medium. The particles were allowed to fall freely from a height of 30 cm above the sample center and impact the superhydrophobic surface. After every 20 g of sand impact mass, the CA and RA of the sample surface were measured until the cumulative sand mass reached 100 g [34].

2.8. Electrochemical Test

The electrochemical tests of O-C and SHP-C were conducted in a 3.5 wt% NaCl aqueous solution using an electrochemical workstation (CHI600E, Shanghai Chenhua Instrument Co., Ltd., Shanghai, China). A three-electrode configuration was employed, consisting of a counter electrode (platinum electrode), a reference electrode (saturated calomel electrode), and an iron wire embedded in each O-C or SHP-C mortar specimen as the working electrode [35]. The iron wire had a diameter of 2 mm and was embedded with a cover depth of 2.5 mm. The embedded iron wire was not directly exposed to the electrolyte, while the mortar surface area exposed to the electrolyte was controlled at 1 cm^2. Three independent specimens were tested for each group. Before electrochemical testing, the specimens were immersed in the 3.5 wt% NaCl solution for 24 h. The electrolyte volume was 250 mL, and all measurements were conducted at 25 ± 1 °C. After the 24 h immersion period, the specimens were allowed to stabilize for 30 min until a relatively stable open-circuit potential (OCP) was obtained. Potentiodynamic polarization measurements were then performed at a scan rate of 1 $mV \cdot s^{-1}$ over a potential range of −0.25 to + 0.25 V relative to the OCP.

3. Results and Discussion

3.1. Surface Morphology and Chemical Composition

Figure 2 shows the macroscopic surface morphology, microstructures, and proposed reaction mechanism between stearic acid and the cement surface. As shown in Figure 2a, after removal of the nylon mesh, a relatively regular and continuous grid-like protru-

sion/depression structure was formed on the SHP-C surface. This surface texture originated from the topographical replication of the 300 μm nylon mesh template during the hardening process of the cementitious material. Further SEM images showed that abundant cement hydration products and fine particles were distributed on the surface of the micrometer-scale texture generated by the template, thereby constructing a rough surface with multiscale hierarchical features. Such a hierarchical rough structure provides an essential physical foundation for achieving superhydrophobicity [36,37]. As observed from the droplet morphology in Figure 2a, water droplets exhibited a nearly spherical shape on the SHP-C surface, with a CA of approximately 156° ± 0.9°. According to the Cassie–Baxter model, the rough structure facilitates air entrapment beneath the droplet, forming a solid–liquid–air composite interface, thereby reducing the actual solid–liquid contact area and enhancing the apparent contact angle. In addition to surface roughness, the low surface free energy derived from the introduction of stearic acid is another crucial factor contributing to the superhydrophobicity of SHP-C. As illustrated in Figure 2b, calcium-containing active sites, such as Ca-OH groups, exist on the surface of cement particles. The carboxyl groups of stearic acid molecules may undergo adsorption, coordination, or interfacial reactions with these calcium-containing sites, constructing a stable hydrophobic organic layer. Meanwhile, the long-chain alkyl groups ($CH_3(CH_2)_{16}$–) are oriented outward from the material surface, thereby forming an organic hydrophobic layer with a relatively low surface free energy [38]. Therefore, the superhydrophobic behavior of SHP-C can be attributed to the combined effects of two factors. On the one hand, the long hydrocarbon chains of STA contribute to lowering the surface free energy of the mortar. On the other hand, the nylon mesh template, together with the surface features of the cementitious matrix, provides surface roughness that contributes to the larger water contact angle of SHP-C. We also investigated the effect of different STA dosages (0.5 g, 1.0 g, 1.5 g, 2.0 g, 2.5 g, and 3.0 g) on the wettability of STA-modified cement powder (Figure 2c). For the contact angle measurements, the modified cement powders were compacted to form a flat surface before testing (Figure 2d). The water contact angle of the compacted modified cement powder increased as the STA dosage increased from 0.5 g to 2.0 g and then decreased with a further increase to 2.5 g and 3.0 g. The maximum water contact angle was obtained at an STA dosage of 2.0 g. In addition, four groups were compared: cement mortar without STA modification or template molding (O-C), cement mortar without STA modification but with template molding (T-C), STA-modified cement mortar without template molding (S-C), and STA-modified cement mortar with template molding (SHP-C). As shown in Figure 2e, O-C and T-C exhibited hydrophilic behavior, whereas STA modification substantially increased the water contact angle of S-C. The combination of STA modification and template molding further increased the water contact angle, resulting in the superhydrophobic SHP-C surface. These results clearly distinguish the individual and combined contributions of STA modification and template-induced surface structuring to the surface wettability.

3.2. Self-Cleaning and Antifouling Performance

A typical characteristic of superhydrophobic surfaces is their self-cleaning ability, similar to the "lotus effect" [39]. Figure 3 compares the removal behavior of chalk dust contaminants on the surfaces of O-C and SHP-C. For O-C, when water droplets contacted the chalk dust-covered surface, they tended to spread or penetrate into the surface pores because O-C had a relatively high surface energy, showing hydrophilicity. Meanwhile, the chalk dust further adhered to the material surface under the wetting effect of water. Therefore, even when water droplets moved along the inclined surface, a considerable amount of contaminant remained. In contrast, water droplets on the SHP-C surface maintained a nearly spherical shape throughout the cleaning process. At a small inclination angle

of approximately 15°, the droplets could roll off and carry away the chalk dust particles from the SHP-C surface. As water droplets continuously rolled across the surface, the contaminated area gradually decreased and eventually returned to an essentially clean state (Video S1). This result can be attributed to the small solid–liquid contact area and weak interfacial adhesion of SHP-C. Water droplets in the Cassie–Baxter state mainly contact the tops of the rough structures, while a large amount of air is retained beneath the droplets. The low solid–liquid adhesion of the SHP-C surface facilitates droplet rolling at a small inclination angle and enables the droplets to carry away the chalk dust particles from the surface, resulting in self-cleaning.

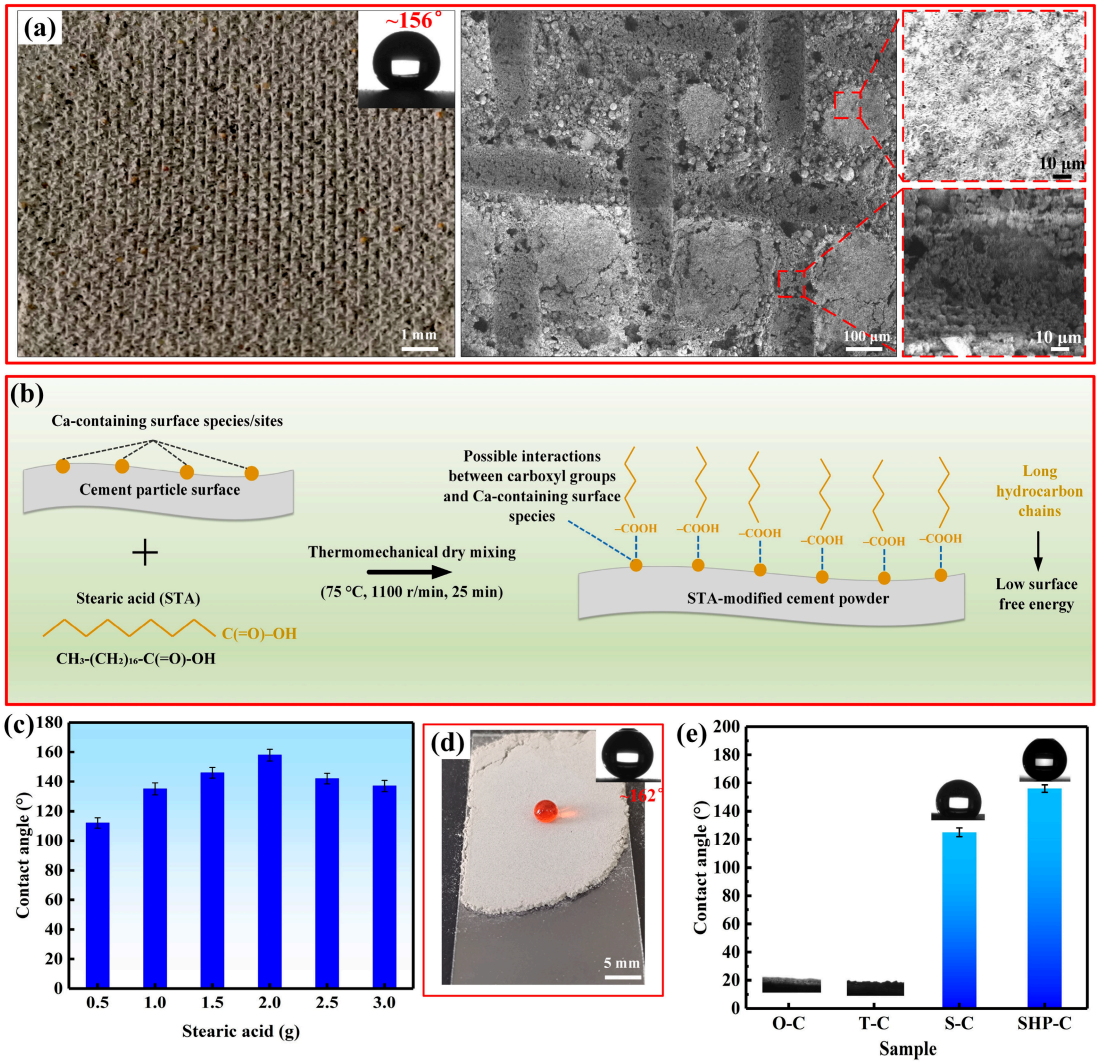

Figure 2. Surface microstructure of SHP-C and wetting of STA-modified cement powder. (**a**) Image, CA, and SEM images of SHP-C. (**b**) Schematic illustration of the proposed dry modification of cement powder with stearic acid. (**c**) Effect of STA dosage on the water contact angle of STA-modified cement powder. (**d**) Image of a water droplet on compacted STA-modified cement powder. (**e**) Comparison of the contact angles of O-C, T-C, S-C, and SHP-C.

In practical applications, building materials may be exposed to various liquid contaminants, such as rainwater, muddy water, and other water-soluble liquids [40]. Therefore, evaluation based solely on the contact angle of deionized water is insufficient to comprehensively assess the practical applicability of SHP-C. Figure 4a shows the droplet contact angles of tea, ink, simulated seawater, muddy water, cola, coffee, milk, and juice on the SHP-C surface. Despite obvious differences in surface tension, viscosity, and chemical

composition among these liquids, the droplets remained essentially spherical on the SHP-C surface, indicating its excellent repellency to a broad range of water-based liquids. The contact angles of all tested liquids on the SHP-C surface remained above 150 ° ± 0.7°, and the rolling angles were less than 10° ± 0.4° (Figure 4b). Among them, even for relatively complex liquids containing sugars, proteins, or suspended particles, such as coffee, milk, and juice, SHP-C still maintained a distinct low-adhesion wetting state. This indicates that the surface exhibits relatively stable low-adhesion wetting characteristics for water-based contaminant liquids with different compositions. Figure 4c further compares the contamination conditions on the surfaces of O-C and SHP-C after different liquid droplets fell onto them. All liquids on the SHP-C surface could rapidly shed from the sample, resulting in a clean surface (Video S2). In contrast, liquids on the O-C surface tended to be absorbed or retained, leaving obvious contamination marks. For example, ink, muddy water, coffee, and juice produced pronounced color staining on the O-C surface, whereas the SHP-C surface remained clean. This result is of potential value, especially for cement-based components in building facades, road infrastructure, and marine environments, because reducing contaminant retention can not only maintain the appearance of building facades but also potentially reduce the continuous contact of saline solutions and other aggressive media with the cement mortar.

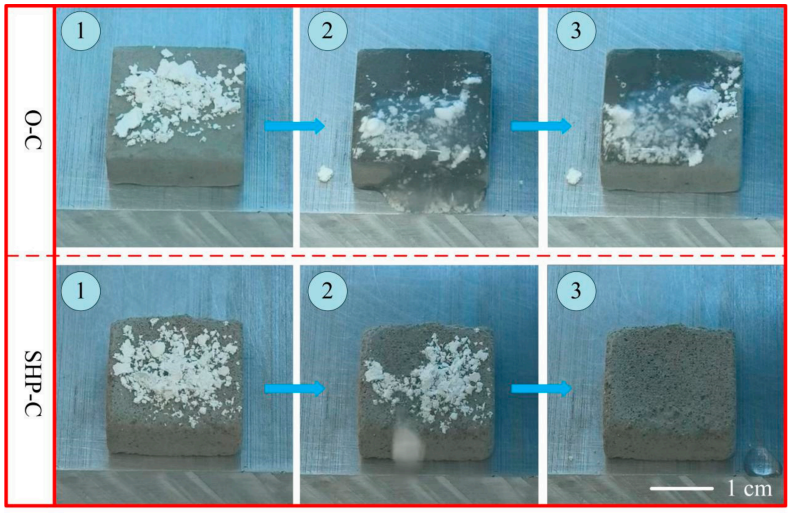

Figure 3. Self-cleaning test processes of chalk dust on the surfaces of O-C and SHP-C.

3.3. Mechanical Robustness

Mechanical robustness is one of the key factors limiting the practical application of superhydrophobic materials [41]. Once the micro/nanostructures are damaged by friction, the liquid may transfer from the Cassie–Baxter state to the Wenzel state, resulting in a decreased contact angle and an increased rolling angle. Figure 5a shows the sandpaper abrasion test process, where the sample was horizontally moved on 800# sandpaper under a constant load of 200 g (Video S3). Figure 5b presents the variations in the CA and RA of SHP-C with increasing abrasion cycles. Before abrasion, SHP-C exhibited a CA of approximately 156° ± 0.9° and an RA of approximately 6° ± 0.5°. As the number of abrasion cycles increased, the contact angle decreased only slowly, while the rolling angle increased slightly. After 10 abrasion cycles (about 200 cm), the CA remained at about 154° ± 0.8°, and the RA remained below 10° ± 0.6°. These results indicate that SHP-C can maintain its superhydrophobic state even under sustained abrasion. This may be attributed to the fact that sandpaper abrasion continuously removes the surface layer of SHP-C, gradually reducing the sample thickness and causing progressive damage to the regular microstructures constructed by the template. However, because the hydrophobically

modified cement is distributed throughout the cement mortar, the newly exposed regions still have microstructures with low-surface-energy characteristics after the surface layer is removed (Figure 5c). In addition, the grooves and irregular microstructures generated during sandpaper abrasion may enable the surface to maintain its roughness. Therefore, the hydrophobic components in the matrix and the rough structures remaining or newly formed after abrasion together facilitate the maintenance of the superhydrophobic state of SHP-C.

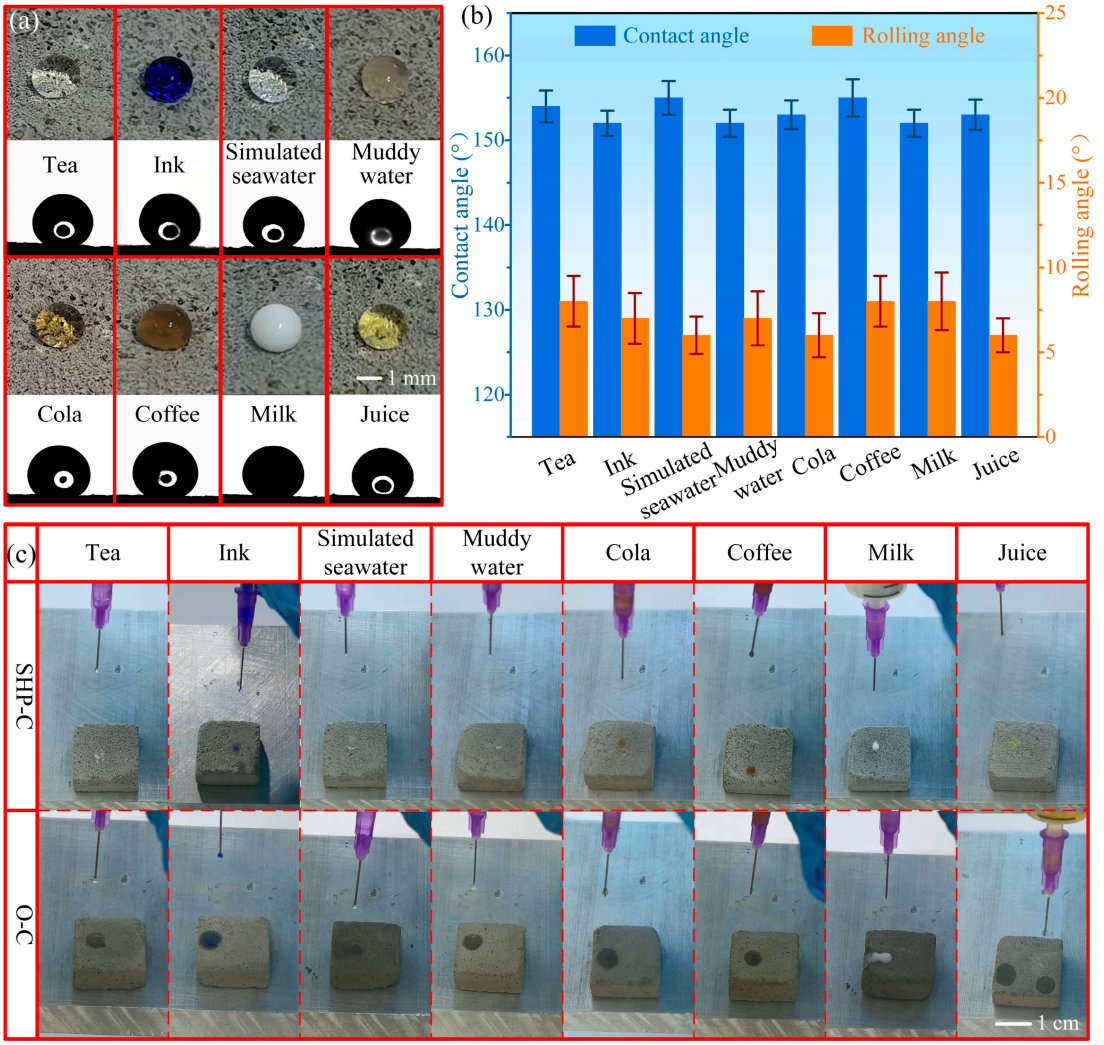

Figure 4. Antifouling performance of SHP-C. (**a**) Different water-soluble liquids on SHP-C. (**b**) Contact angles and rolling angles of different water-soluble liquids on SHP-C. (**c**) Comparison of contamination behavior between SHP-C and O-C.

Besides abrasion, cement mortar may also be subjected to persistent impact from solid particles. Therefore, a falling-sand impact test was further conducted to evaluate the mechanical robustness of SHP-C. As shown in Figure 6a and Video S4, the sample was fixed on a platform with a 20° inclination angle. Sea sand with a particle size of about 1 mm was allowed to fall freely from a height of 30 cm to impact the SHP-C surface. It can be seen that the CA and RA showed almost no significant change as the cumulative mass of impacting sand particles increased from 0 to 100 g (Figure 6b). The initial CA was approximately 156° ± 0.9°, and it remained at approximately 153° ± 0.7° after impact by 100 g of sand particles. Meanwhile, the rolling angle remained within a low range. This indicates that although sand particle impact caused certain damage to the surface rough structures, it was

insufficient to cause a substantial transition of the droplets to the high-adhesion Wenzel state. The sandpaper abrasion and sand impact tests demonstrate that SHP-C exhibits good stability against different forms of mechanical damage, highlighting its potential for practical applications in outdoor environments.

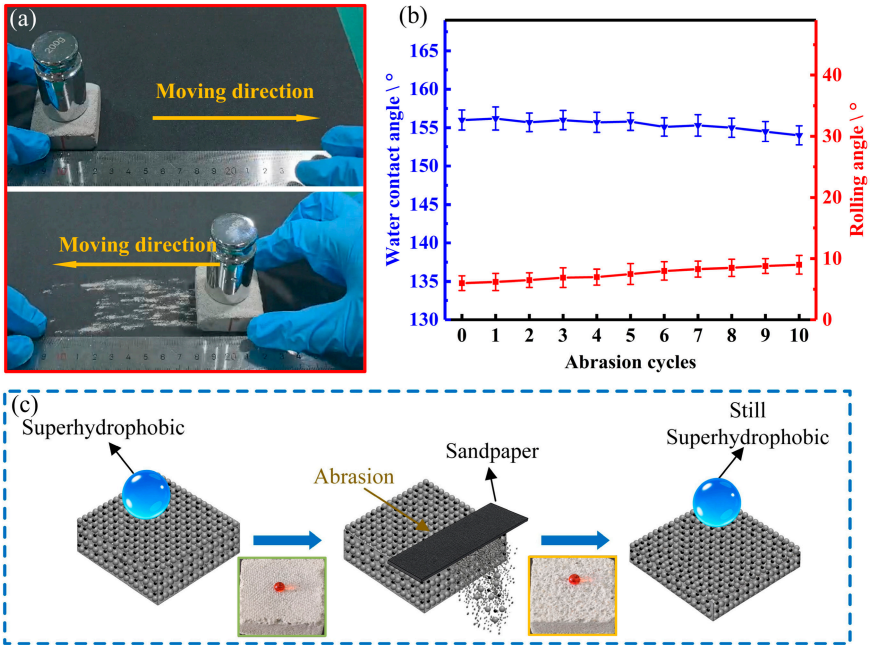

Figure 5. Sandpaper abrasion performance of SHP-C. (**a**) Abrasion test processes. (**b**) Variation in CA and RA with abrasion cycles. (**c**) Schematic illustration of the abrasion process of SHP-C.

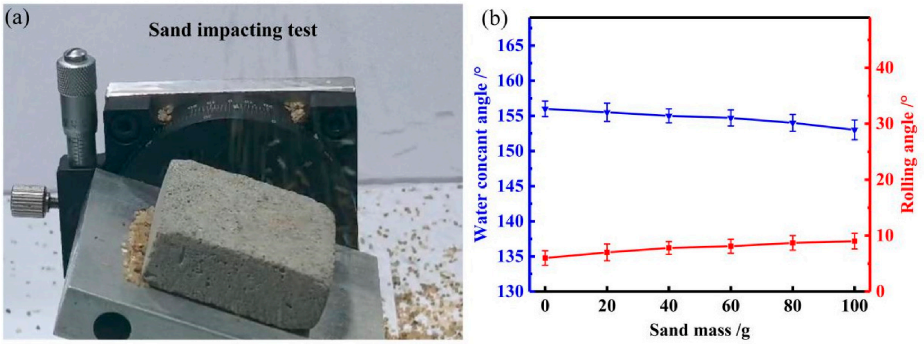

Figure 6. Sand impact performance of SHP-C. (**a**) Image of the sand impact test. (**b**) Variation in CA and RA with sand mass.

3.4. Corrosion Resistance

The ingress of water and water-soluble corrosive species into porous cementitious materials is an important prerequisite for the deterioration of cement mortar structures. Theoretically, a superhydrophobic interface can act as a physical barrier at the material surface by reducing liquid-solid contact and suppressing water penetration, thereby lowering the transport rate of aggressive ions [42,43]. Figure 7 shows the potentiodynamic polarization curves of O-C and SHP-C, where the corrosion current density (I_{corr}) and corrosion potential (E_{corr}) were obtained by Tafel extrapolation. The I_{corr} and E_{corr} values of O-C were 3.925×10^{-4} A·cm^{-2} and -1.089 V, respectively, while those of SHP-C were 1.745×10^{-5} A·cm^{-2} and -0.908 V, respectively. Compared with O-C, SHP-C exhibited an approximately 22.5 times lower corrosion current density, indicating that the electrochemical corrosion reaction was significantly suppressed. Therefore, superhydrophobic treatment can effectively improve the corrosion resistance of cement mortar. The underlying mecha-

nism may involve two aspects. On the one hand, the low-surface-energy rough interface significantly reduces the direct contact area between the electrolyte and the material. On the other hand, the air trapped within the rough structures and the reduced solid–liquid contact area may help inhibit electrolyte wetting and retard the penetration of Cl^- ions and moisture into the surface pores. Consequently, the continuous transport channels of the electrolyte required for electrochemical reactions are disrupted, ultimately reducing the corrosion activity of the material.

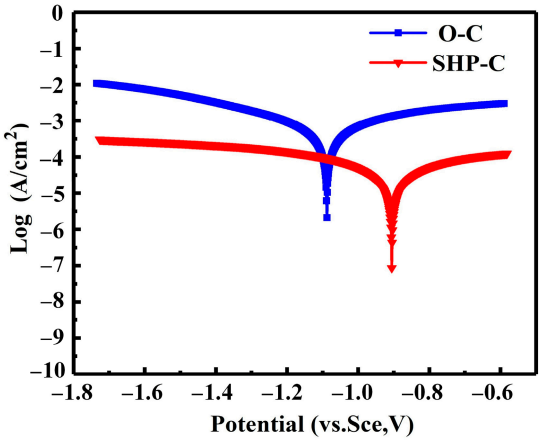

Figure 7. Potentiodynamic polarization curves of O-C and SHP-C.

3.5. Appearance Tunability and Literature Comparison

In addition to water-repellent and durability performance, the appearance of building materials is also an important factor influencing practical applications. Figure 8 demonstrates the compatibility of the proposed preparation strategy with cementitious systems of different colors. The colored samples were prepared by adding water-based colorants of different colors to the mortar mixtures. By adjusting the color of the added water-based colorant, different visual effects such as red, gray, and light yellow can be obtained, while water droplets still maintain an essentially spherical shape on the surfaces of different samples. This phenomenon indicates that the adopted superhydrophobic design strategy exhibits certain tunability in surface appearance and potential for decorative applications, which means that the hydrophobic function of the material surface is not restricted to a single-color cement mortar. Therefore, this strategy is expected to be applied in the future to buildings, decorative cement mortar, landscape components, pedestrian pavements, and other cement mortar materials that require both decorative and functional properties.



Figure 8. Superhydrophobic cement mortar with different color appearances.

In addition, we compared this work with the previous literature in terms of modification strategies, solvent/auxiliary materials, wettability, mechanical durability, and corrosion resistance [29,38,44–47]. Compared with previous studies, this work achieves superhydrophobicity using a solvent-free dry-modification strategy. The treated mor-

tar also exhibits good mechanical durability and corrosion resistance, demonstrating the effectiveness of the proposed method (Table 1).

Table 1. Comparison of representative superhydrophobic cementitious materials reported in previous studies and this work.

References	Modification Strategy	Solvent/Auxiliary Material	Ca (°)	Ra (°)	Mechanical Durability	Corrosion Resistance I_{corr} (a·cm^{-2})
[29]	STA-modified oyster shell powder as sand replacement	Ethanol, OSP	95.2	/	/	/
[38]	STA incorporation + Cu-mesh texturing	Ethanol, Cu mesh	159	5	CA > 150° after 60 s polishing	/
[44]	STA-modified iron ore tailings as sand replacement	Ethanol, IOTs	124	/	/	1.45×10^{-6}
[45]	Direct incorporation of STA solution into mortar	Ethanol	154	/	/	3.13×10^{-6}
[46]	STA/ZnO/epoxy surface coating	Ethanol, ZnO, epoxy	164	4.6	CA of 160° after 300 cm abrasion	/
[47]	STA-modified zeolite surface coating	Zeolite	156	<10	/	1.02×10^{-5}
This work	Thermomechanical dry modification of cement with STA	Solvent-free	156	6	CA ~ 154° after 200 cm abrasion	1.75×10^{-5}

4. Conclusions

In this work, we propose a method for preparing superhydrophobic cement mortar by combining dry pre-modification of cement powder with stearic acid (STA) and nylon mesh template molding. The prepared SHP-C exhibited excellent superhydrophobicity, self-cleaning performance, antifouling properties, mechanical durability, and improved electrochemical corrosion performance of the embedded iron electrode. The SHP-C surface exhibited a CA of approximately 156° ± 0.9° and an RA of approximately 6° ± 0.5°. Surface morphology and the proposed reaction mechanism indicated that the long hydrocarbon chains of STA contributed to lowering the surface free energy, while the nylon mesh template introduced surface roughness that contributed to the high apparent water contact angle. SHP-C can remove solid contaminants from the surface through water droplets and prevent the adhesion of water-soluble liquids, such as tea, ink, simulated seawater, muddy water, cola, coffee, milk, and juice, showing good self-cleaning and antifouling performance. Sandpaper abrasion and sand impact tests demonstrated that SHP-C could retain its superhydrophobicity after continuous abrasion and particle impact, exhibiting good mechanical stability. After 10 sandpaper abrasion cycles, the CA remained approximately 154° ± 0.8°, and the RA remained below 10° ± 0.6°. After a cumulative sand impact of 100 g, the CA remained approximately 153° ± 0.7°. During abrasion processes, although the surface layer was gradually removed, the newly exposed regions could still maintain certain hydrophobic characteristics. The polarization curve results showed that the corrosion current density (I_{corr}) of the embedded iron electrode decreased from 3.925×10^{-4} A·cm^{-2} for O-C to 1.745×10^{-5} A·cm^{-2} for SHP-C, a decrease of 22.5 times. These results indicate improved electrochemical corrosion performance of the embedded iron electrode in SHP-C under the investigated conditions. In addition, the method exhibited certain color and appearance tunability. Based on the above findings, the proposed preparation method for superhydrophobic cement mortar features simple processing and avoids the use of fluorinated low-surface-energy agents, demonstrating potential application in the surface protection and functionalization of cement-based infrastructure.

Supplementary Materials: The following supporting information can be downloaded at https://www.mdpi.com/article/10.3390/coatings16101198/s1, Video S1: Self-cleaning test; Video S2:

Rolling processes of water-soluble droplets of SHP-C; Video S3: Sandpaper abrasion test; Video S4: Sand impact test.

Author Contributions: Conceptualization, Y.Z. and S.L.; methodology, Y.Z. and Z.G.; validation, Y.Z., H.C. and H.W.; investigation, Y.Z., D.Y. and S.L.; data curation, Y.Z., H.C. and H.W.; writing—original draft preparation, Y.Z. and S.L.; writing—review and editing, D.Y. and S.L.; visualization, H.C. and S.L.; supervision, S.L. and D.Y.; funding acquisition, S.L. All authors have read and agreed to the published version of the manuscript.

Funding: This research was funded by the Science and Technology Development Program Project of Jilin Province, grant number YDZJ202501ZYTS366.

Institutional Review Board Statement: Not applicable.

Informed Consent Statement: Not applicable.

Data Availability Statement: Data are contained within this article.

Conflicts of Interest: The authors declare no conflicts of interest.

References

1. Haller, T.; Scherb, S.; Beuntner, N.; Thienel, K.-C. Renewable construction with lightweight concrete—Reclaimed recycled material systems with CO_2-absorption. *Constr. Build. Mater.* **2025**, *466*, 140339. [CrossRef]
2. Ma, J.; Yang, Q.; Peng, X.; Xia, K. Review on Durability Deterioration and Mitigation of Concrete Structures. *Coatings* **2025**, *15*, 982. [CrossRef]
3. Nilimaa, J. Smart materials and technologies for sustainable concrete construction. *Dev. Built Environ.* **2023**, *15*, 100177. [CrossRef]
4. Yan, D.; Lv, S.; Mao, C.; Mou, X.; Zhai, Y.; Liu, Q. A concrete with superhydrophobic and photothermal coating for water repellent and efficient anti-icing. *Constr. Build. Mater.* **2026**, *542*, 147971. [CrossRef]
5. Monteiro, P.J.M.; Miller, S.A.; Horvath, A. Towards sustainable concrete. *Nat. Mater.* **2017**, *16*, 698–699. [CrossRef]
6. Zhou, X.; Li, M.; Guan, X.; Shi, J. Insights into the enhanced corrosion resistance of carbon steel in a novel low-carbon concrete with red mud and phytic acid. *Corros. Sci.* **2022**, *211*, 110903. [CrossRef]
7. Portela, G.M.; Pacheco, F.; Ehrenbring, H.Z.; Christ, R.; Tutikian, B.; Mancio, M. Effects of Different Coatings on Concrete Elements Due to Chloride Ion Penetration. *Coatings* **2025**, *15*, 46. [CrossRef]
8. Yan, D.; Lin, J.; Chen, Y.; Yang, X.; Lu, Y.; Song, J. High-Efficiency Water Collection of Superhydrophobic Condensation Absorber. *Adv. Sci.* **2025**, *12*, e2417024. [CrossRef]
9. Lv, S.; Tao, C.; Yan, D.; Mou, X.; Mao, C.; Zhai, Y.; Liu, Q.; Xiao, S. Biomimetic water-repellent slippery coating for engineering metal surfaces. *Prog. Org. Coat.* **2026**, *219*, 110354. [CrossRef]
10. Polishchuk, I.; Prudnikov, E.; Abu-Hamad, H.; Ben-Arie, N.; Sklar, J.; Kellermeier, M.; Schneider, C.; Rueckel, M.; Tauber, F.; Revert, M.A.I.; et al. SafeWax: A Bio-Inspired Multifunctional Coating for Sustainable Crop Protection. *Small* **2025**, *21*, e05360. [CrossRef]
11. Zhang, C.; Wu, S.; Wang, X.; Zhang, B.; Song, J. Compound eye inspired multi-scale superhydrophobic hemispherical array for preventing supercooled water droplet freezing. *Chem. Eng. J.* **2026**, *544*, 178066. [CrossRef]
12. Lin, J.; Wang, X.; Wang, H.; Sun, Z.; Yan, D.; Song, J. High drag reduction by spontaneous capture and transportation of bubbles. *Nanoscale* **2025**, *17*, 10892–10900. [CrossRef]
13. Yan, D.; Lu, Y.; Lin, J.; Li, W.; Song, J. Enhancing water transportation capacity by asymmetrical patterned surface with super-wettability. *Appl. Phys. Lett.* **2024**, *125*, 071601. [CrossRef]
14. Wang, Y.; Sun, Y.; Xue, Y.; Sui, X.; Yuan, B.; Wang, Y.; Liang, W. Functional surfaces with reversibly switchable wettability: Fundamentals, progresses, applications and challenges. *Prog. Org. Coat.* **2024**, *188*, 108167. [CrossRef]
15. Wang, Y.; Xue, Y.; Wang, Y.; Yuan, B.; Zheng, Y.; Liang, W.; Sun, Y.; Sui, X. Multi-response controllable microstructured superhydrophobic surfaces for full-process dynamic anti-icing and de-icing. *Compos. Sci. Technol.* **2025**, *267*, 111183. [CrossRef]
16. Zhang, Z.; Gao, N.; Zhang, F.; Liu, L.; Chen, Y. Photothermal-driven water-gliding microrobots based on fully integrated flexible sensors with heterogeneous wettability. *Soft Sci.* **2025**, *5*, 15. [CrossRef]
17. Chen, Y.; Li, K.; Yan, D.; Liu, R.; Song, J. 2D Water Turbine Based on Extreme Wettability Surface. *Surf. Interfaces* **2026**, *97*, 110057. [CrossRef]
18. Lv, X.-S.; Cao, W.-X.; Yio, M.; Ji, W.-Y.; Lu, J.-X.; She, W.; Poon, C.S. High-performance lightweight foam concrete enabled by compositing ultra-stable hydrophobic aqueous foam. *Cem. Concr. Compos.* **2024**, *152*, 105675. [CrossRef]
19. Shen, C.; Zhu, Y.; Shi, W.; He, K.; Xiao, X.; Xu, X.; Shi, J.; Xu, G. Mechanically stable superhydrophobic surface on cement-based materials. *Chem. Phys.* **2020**, *538*, 110912. [CrossRef]

20. Lv, X.-S.; Cao, W.-X.; Yio, M.; Lu, J.-X.; Poon, C.S. 3D superhydrophobic lightweight foam concrete designed via in-situ foaming and self-assembled silicone microfilms. *Chem. Eng. J.* **2023**, *478*, 147390. [CrossRef]
21. Song, J.; Zhao, D.; Han, Z.; Xu, W.; Lu, Y.; Liu, X.; Liu, B.; Carmalt, C.J.; Deng, X.; Parkin, I.P. Super-robust superhydrophobic concrete. *J. Mater. Chem. A* **2017**, *5*, 14542–14550. [CrossRef]
22. Song, J.; Li, S.; Zhao, C.; Lu, Y.; Zhao, D.; Sun, J.; Roy, T.; Carmalt, C.J.; Deng, X.; Parkin, I.P. A superhydrophilic cement-coated mesh: An acid, alkali, and organic reagent-free material for oil/water separation. *Nanoscale* **2017**, *10*, 1920–1929. [CrossRef]
23. Song, J.; Li, Y.; Xu, W.; Liu, H.; Lu, Y. Inexpensive and non-fluorinated superhydrophobic concrete coating for anti-icing and anti-corrosion. *J. Colloid Interface Sci.* **2019**, *541*, 86–92. [CrossRef]
24. Xu, K.; Ren, S.; Song, J.; Liu, J.; Liu, Z.; Sun, J.; Ling, S. Colorful superhydrophobic concrete coating. *Chem. Eng. J.* **2021**, *403*, 126348. [CrossRef]
25. Ren, S.; Chen, Y.; Xu, K.; Liu, J.; Sun, J.; Zhao, D.; Ling, S.; Song, J.; Hua, S. Maintenance of superhydrophobic concrete for high compressive strength. *J. Mater. Sci.* **2020**, *56*, 4588–4598. [CrossRef]
26. Sultan, U.; Walter, T.; Wachter, C.; Swart, L.; Vogel, N. A Supraparticle-Based Approach to Robust Biomimetic Superhydrophobic Coatings. *Small* **2025**, *21*, e05850. [CrossRef]
27. Wang, D.; Sun, Q.; Hokkanen, M.J.; Zhang, C.; Lin, F.-Y.; Liu, Q.; Zhu, S.-P.; Zhou, T.; Chang, Q.; He, B.; et al. Design of robust superhydrophobic surfaces. *Nature* **2020**, *582*, 55–59. [CrossRef]
28. Lv, S.; Liu, F.; Yang, Z.; Han, J.; Zhai, Y.; Mao, C.; Yan, D. Superhydrophobic surface with rice leaf structures fabricated by laser processing. *Opt. Laser Technol.* **2025**, *189*, 113072. [CrossRef]
29. Song, Q.; Wang, Q.; Xu, S.; Mao, J.; Li, X.; Zhao, Y. Properties of water-repellent concrete mortar containing superhydrophobic oyster shell powder. *Constr. Build. Mater.* **2022**, *337*, 127423. [CrossRef]
30. Ji, J.; Lin, X.; Hu, Y.; Ming, P.; Ren, W.; Song, J. Additive manufacturing of microstructures by cold-liquid silicone oil constrained meniscus-confined electrodeposition. *Addit. Manuf.* **2026**, *127*, 105268. [CrossRef]
31. Wang, Z.; Duan, Z.; Wang, S.; Li, Y.; Zhou, Y.; Liu, J.; Liu, X. Influence of cold plasma on material removal behavior during diamond grit scratching single crystal silicon. *Colloids Surf. A Physicochem. Eng. Asp.* **2024**, *705*, 135630. [CrossRef]
32. Pan, W.; Wang, Q.; Ma, J.; Xu, W.; Sun, J.; Liu, X.; Song, J. Solid-Like Slippery Coating with Highly Comprehensive Performance. *Adv. Funct. Mater.* **2023**, *33*, 2302311. [CrossRef]
33. Zhang, W.; Wang, D.; Sun, Z.; Song, J.; Deng, X. Robust superhydrophobicity: Mechanisms and strategies. *Chem. Soc. Rev.* **2021**, *50*, 4031–4061. [CrossRef]
34. Tang, Y.; Yang, X.; Li, Y.; Lu, Y.; Zhu, D. Robust Micro-Nanostructured Superhydrophobic Surfaces for Long-Term Dropwise Condensation. *Nano Lett.* **2021**, *21*, 9824–9833. [CrossRef]
35. Sun, Y.; Liu, J.; Ming, P.; Zhao, D.; Song, J. Wire electrochemical etching of superhydrophobic 304 stainless steel surfaces based on high local current density with neutral electrolyte. *Appl. Surf. Sci.* **2022**, *571*, 151269. [CrossRef]
36. Zang, X.; Bian, J.; Ni, Y.; Zheng, W.; Zhu, T.; Chen, Z.; Cao, X.; Huang, J.; Lai, Y.; Lin, Z. A Robust Biomimetic Superhydrophobic Coating with Superior Mechanical Durability and Chemical Stability for Inner Pipeline Protection. *Adv. Sci.* **2024**, *11*, e2305839. [CrossRef]
37. Balordi, M.; Cammi, A.; Casali, A.; Pini, F.; de Magistris, G.S. On the Hydrophobicity, Superhydrophobicity and Icephobicity of Etched Aluminum Surfaces. *Coatings* **2025**, *15*, 1328. [CrossRef]
38. Lei, L.; Wang, Q.; Xu, S.; Wang, N.; Zheng, X. Fabrication of superhydrophobic concrete used in marine environment with anti-corrosion and stable mechanical properties. *Constr. Build. Mater.* **2020**, *251*, 118946. [CrossRef]
39. Tu, S.; Zhang, L.; Zhang, W.; Feng, J. Waterborne Recoatable Transparent Superhydrophobic Coatings with Excellent Self-Cleaning and Anti-Dust Performance. *Small* **2025**, *21*, e2410171. [CrossRef]
40. Chen, G.; Xu, Y.; Zhang, B.; Zhou, Y.; Wang, S.; Meng, Y.; Huang, L.; Song, J. Superhydrophobic coating with super-high adhesive strength to substrate. *Mater. Lett.* **2023**, *351*, 135084. [CrossRef]
41. Lu, Y.; Sathasivam, S.; Song, J.; Crick, C.R.; Carmalt, C.J.; Parkin, I.P. Repellent materials. Robust self-cleaning surfaces that function when exposed to either air or oil. *Science* **2015**, *347*, 1132–1135. [CrossRef]
42. Chen, F.; Wang, Y.; Tian, Y.; Zhang, D.; Song, J.; Crick, C.R.; Carmalt, C.J.; Parkin, I.P.; Lu, Y. Robust and durable liquid-repellent surfaces. *Chem. Soc. Rev.* **2022**, *51*, 8476–8583. [CrossRef]
43. Nuñez, L.E.V.; Cornejo-Monroy, D.; Sánchez-Santamaria, B.; Arias-Cerón, J.S.; Villanueva-Montellano, A.; López-Ibarra, A.A.; Jáquez-Muñoz, J.M. Study of Al7075 Localized Corrosion Inhibition by a SiO_2 Superhydrophobic Coating Employing an Electrochemical Noise Technique. *Coatings* **2025**, *15*, 131. [CrossRef]
44. Wang, M.; Wang, Q.; Mao, J.; Xu, S.; Shi, Z. Study on water-repellent and corrosion-resistant properties of cement mortar using superhydrophobic iron ore tailings. *J. Build. Eng.* **2022**, *62*, 105360. [CrossRef]
45. Zhao, Y.; Lei, L.; Wang, Q.; Li, X. Study of superhydrophobic concrete with integral superhydrophobicity and anti-corrosion property. *Case Stud. Constr. Mater.* **2023**, *18*, e01899. [CrossRef]

46. Han, Y.; Liu, J.; Xia, X.; Yin, J. Preparation of a Stable Superhydrophobic Mortar Surface Using a One-Step Method. *Langmuir* **2023**, *39*, 16543–16553. [CrossRef]
47. Xu, S.; Wang, Q.; Zhuo, X.; Wang, N. Green Fabrication of Superhydrophobic Zeolite Coating on Cement-Based Material Surfaces to Improve Water-Resistant and Anticorrosion Properties. *J. Mater. Civ. Eng.* **2024**, *36*, 114169. [CrossRef]

Disclaimer/Publisher's Note: The statements, opinions and data contained in all publications are solely those of the individual author(s) and contributor(s) and not of MDPI and/or the editor(s). MDPI and/or the editor(s) disclaim responsibility for any injury to people or property resulting from any ideas, methods, instructions or products referred to in the content.